Research Square

Preprints are preliminary reports that have not undergone peer review.
They should not be considered conclusive, used to inform clinical practice,
or referenced by the media as validated information.

Evidence for Kondo-like Scattering in Zr/Cu-Substituted Bi-2223 High-Temperature Superconductors

Fatemeh Poshtibanasl
Alzahra University
Vahid Daadmehr
daadmehr@alzahra.ac.ir
Alzahra University
Fatemeh Shahbaz Tehrani
University of Tehran
Zahra Asghari
Alzahra University
Sadaf Vafajoo
Alzahra University

Article

Keywords: High-temperature cuprate superconductors, non-magnetic substitution, Kondo-like scattering, resistivity anomaly, spin fluctuations

Posted Date: November 25th, 2026

DOI: https://doi.org/10.21203/rs.3.rs-11674503/v1

License: This work is licensed under a Creative Commons Attribution 4.0 International License.
Read Full License

Additional Declarations: No competing interests reported.

Evidence for Kondo-like Scattering in Zr/Cu-Substituted Bi-2223 High-Temperature Superconductors

Fatemeh Poshtibanasl[1], Vahid Daadmehr [1]* , Fatemeh Shahbaz Tehrani [2], Zahra Asghari[1], and Sadaf Vafajoo[1]

1. Magnet & Superconducting Research Lab, Physics Faculty, Alzahra University, Tehran, 1993893973, IRAN

2. Nanophysics Research Laboratory, Dept. of Physics, University of Tehran, Tehran 14395-547, IRAN

**Corresponding author: daadmehr@alzahra.ac.ir*

Abstract

High-temperature cuprate superconductors (HTCS) exhibit complex electronic states in which superconductivity, magnetic fluctuations, and anomalous charge transport coexist. Low-temperature resistivity anomalies observed in these materials may originate from several competing mechanisms, including vortex dynamics, and spin-dependent scattering processes. In this work, we investigate the transport properties of lightly Zr/Cu-substituted Bi-2223 superconductors with a nominal composition of $Bi_{1.66}Pb_{0.34}Sr_2Ca_2Cu_{2.998}Zr_{0.002}O_{10+\delta}$ under weak external magnetic fields. Electrical resistivity measurements under magnetic fields of 0.3, 0.4, and 0.65 T reveal a low-temperature logarithmic resistivity contribution in the superconducting low-temperature regime. This behavior is consistent with an additional spin-dependent scattering channel arising from Kondo-like screening of impurity-induced local moments, beyond conventional potential scattering of charge carriers. To identify the origin of

*Corresponding author:

Tel: (+98 21) 85692631 / (+98) 912608 9714

Fax: (+98 21) 88047861

E-mail: daadmehr@alzahra.ac.ir ; daadmehr@gmail.com

https://scholar.google.com/DaadmehrORCID identification number: 0000-0002-0554-3261
E-mail: fatemeh.poshtiban.asl@gmail.com

E-mail: tehrani66@gmail.com ORCID identification number: 0000-0002-6098-3286
E-mail: zahraasghary42@gmail.com

E-mail: sadaf.vafajoo93@gmail.com

this anomaly, the experimental resistivity data are investigated by Kondo effect. Zr^{4+} is intrinsically non-magnetic, but its heterovalent substitution in the Cu-containing lattice can modify the local charge distribution, Cu–O bonding, and electronic states, potentially generating impurity-induced spin fluctuations on neighboring CuO_2 planes. Comparison of the experimentally obtained logarithmic resistivity coefficients with the corresponding Kondo parameters shows qualitative consistency with a Kondo-like scattering contribution. Among the investigated magnetic fields, H = 0.4 T shows the closest correspondence between the experimental and calculated resistivity trends, whereas at 0.65 T the logarithmic coefficients are nearly identical but the curves are offset, suggesting that the relative contribution of spin-dependent scattering depends on the field. These results suggest that Zr-induced modification of the local Cu–O electronic environment may contribute to a weak field-dependent Kondo-like scattering component in the low-temperature regime of Bi-2223 superconductor.

Keywords: High-temperature cuprate superconductors, non-magnetic substitution, Kondo-like scattering, resistivity anomaly, spin fluctuations

1. Introduction

High-temperature cuprate superconductors (HTCS) represent a class of strongly correlated materials [1] in which superconductivity emerges from the electronic structure of the CuO_2 planes [2]. Since the discovery of high-temperature superconductivity in copper oxides [3], considerable attention has been devoted to understanding the interplay between superconducting pairing, magnetic fluctuations, and charge transport in these systems [2, 3]. The CuO_2 planes, which constitute the electronic backbone of cuprate superconductors, exhibit strong correlations and are sensitive to chemical substitutions, structural disorder, and external magnetic field [2, 4]. Unlike conventional superconductors, cuprate materials show a variety of anomalous transport phenomena, particularly at low temperatures, where superconducting fluctuations, vortex dynamics, and electronic correlations may simultaneously contribute to the measured electrical response [5, 6]. Therefore, identifying the microscopic origin of additional resistivity appearing near and below the superconducting transition remains an important challenge in high-temperature superconductivity.

The Kondo effect is a well-established phenomenon arising from the interaction between conduction electrons and localized magnetic moments [7]. In conventional dilute magnetic

alloys, Kondo effect produces a characteristic increase in resistivity with decreasing temperature, which in the perturbative regime is described by a logarithmic temperature dependence, $\rho_{spin} \propto log(T)$ [7, 8]. The Kondo effect has also been extensively studied in strongly correlated materials, particularly in heavy-fermion compounds, where the interplay between localized magnetic moments and itinerant electrons gives rise to characteristic many-body phenomena [9, 10]. Kondo-like scattering has also been discussed in cuprate superconductors containing non-magnetic impurities, where impurity-induced magnetic responses on neighboring Cu sites can interact with the host system's electronic degrees of freedom [11]. However, whether a very dilute non-magnetic substitution can produce a measurable Kondo-like scattering contribution to the electrical resistivity of a high-temperature cuprate remains an open question [11, 12].

Chemical substitution has long been used to tune cuprate superconductors, starting from the Y–Ba–Cu–O phase with $T_c \approx 91$ K [13], and the resulting changes in the electronic structure of the CuO_2 planes can be probed by ARPES [14]. While magnetic dopants can directly introduce localized magnetic moments, non-magnetic substitutions can influence superconducting properties through lattice distortion, charge redistribution, and changes in Cu–O orbital hybridization [12, 15]. In the present system, Zr is considered a possible heterovalent substituent at a Cu site and is assumed to adopt the Zr^{4+} oxidation state, consistent with previous studies reporting tetravalent Zr substitution at Cu sites in cuprate superconductors [16, 17]. This oxidation-state assignment is used as a modeling assumption. The Zr^{4+} ion has a $4d^0$ electronic configuration and therefore does not itself carry an intrinsic local magnetic moment. However, if Zr^{4+} occupies a Cu-containing site, its heterovalent character relative to Cu^{2+} would be expected to perturb the local charge balance and Cu–O bonding environment, potentially modifying the electronic states of neighboring Cu–O sites. Such local perturbations may modify spin polarization and magnetic fluctuations in neighboring Cu–O states, providing a plausible microscopic route to impurity-induced spin-dependent scattering without requiring the Zr^{4+} ion itself to carry a magnetic moment [11, 15]. Therefore, lightly Zr/Cu-substituted Bi-2223 offers a useful system for investigating whether non-magnetic chemical substitution can produce Kondo-like transport signatures via impurity-induced spin-dependent scattering.

An applied magnetic field can influence the superconducting properties of cuprate materials, including shifting the superconducting transition toward lower temperatures, as reported for Bi-2223 superconductors [18]. Previous experimental and theoretical studies have shown that nonmagnetic impurities can induce local magnetic responses in cuprates, which may exhibit

Kondo-like characteristics [11, 19]. Furthermore, theoretical studies have demonstrated that an external magnetic field can induce local magnetic moments around nonmagnetic impurities in metallic cuprates [20]. These findings provide a basis for investigating whether the applied magnetic field influences the impurity-related magnetic response and the possible Kondo-like contribution to the electrical resistivity in the present Zr-substituted Bi-2223 system.

In this work, we investigate the low-temperature transport behavior of lightly Zr/Cu-substituted Bi-2223 superconductor under weak magnetic fields. Structural refinement is used to evaluate whether the experimental diffraction pattern is consistent with a Bi-2223 structural model containing a very small amount of Zr and to assess the associated structural parameters. We analyze the low-temperature resistivity anomaly by considering possible contributions from Kondo-like scattering. By applying the Kondo effect and comparing calculated parameters with experimental logarithmic resistivity coefficients, we assess the possibility of a Kondo-like scattering mechanism in the Zr/Cu-substituted Bi-2223 system. The field dependence of Kondo trend is further examined, with H = 0.4 T showing the closest correspondence between the experimental and calculated parameters among the fields investigated. Our results suggest that weak magnetic fields influence the balance between superconducting correlations and spin-dependent scattering processes in Zr/Cu-substituted Bi-2223 superconductors.

2. Experimental and Structural Characterization

2.1 Sample preparation

To investigate the effect of low-level Zr substitution on the electronic and transport properties of Bi-2223 high-temperature superconductors, we synthesized a lightly Zr/Cu-substituted Bi-2223 ceramic sample using the sol–gel method. Superconducting ceramics have been synthesized by various routes, including solid-state reaction [21, 22] and sol–gel methods [23, 24]. In the present work, the sol–gel route was used, and a related Zr/Cu-substituted Bi-2223 system prepared in this way has previously been investigated by our group [25].

In the present work, the $Bi_{1.66}Pb_{0.34}Sr_2Ca_2Cu_{3-x}Zr_xO_{10+\delta}$ ceramics with a nominal Zr substitution level of x = 0.002 were synthesized using this method. Stoichiometric amounts of $Bi(NO_3)_3.5H_2O$ (99.9%), $Pb(NO_3)_2$ (99.9%), $Sr(NO_3)_2$ (99.9%), $Ca(NO_3)_2.4H_2O$ (99%),

$Cu(NO_3)_2.3H_2O$ (99%), and ZrO_2 (99.9%) were dissolved in deionized water with mild heating, and nitric acid was added to prevent hydroxide precipitation. A separate solution containing polyethylene glycol (PEG) and EDTA (in a 1:1 molar ratio to total metal ions) was prepared and combined with the precursor solution. Ammonia was used to adjust the pH and enhance solubility, and urea was added as a stabilizer. The resulting sol was stirred at 80°C to form a gel [25].

The gel was heated in an oil bath at 120 °C for 10 h, then ramped from 180 to 250 °C over 8 h (average heating rate ≈ 8.75 °C/h), and finally fired at 220–250 °C to obtain a black, foam-like mass. This material was ground into powder for 2 h and calcined at 800 °C for 30 h in a programmable tubular furnace under a continuous flow of air, supplied by an air pump connected to the quartz tube; the calcination was repeated once. The powder was then ground and pressed into 10 mm diameter disks, which were sintered at 835 °C for 200 h under flowing air to obtain dense ceramic samples suitable for structural and superconducting characterization. We reported the morphological and microstructural characteristics of the corresponding low-doped Zr/Cu-substituted Bi-2223 system in detail in our previous work [25].

2.2 Structural analysis

The crystalline structure of the synthesized sample was characterized by X-ray diffraction (XRD) using a PANalytical PW3050/60 diffractometer with Cu Kα radiation (λ = 1.54056 Å), operated at 40 kV and 40 mA. The diffraction patterns were collected with a step size of 0.026°. Rietveld refinement was performed using the Material Analysis Using Diffraction (MAUD) software (version 2.8). The refinement was used to evaluate the crystalline phase and to refine the corresponding crystallographic parameters, including lattice parameters, atomic positions, and site occupancies. The agreement between the experimental and calculated diffraction profiles was evaluated using the refinement residuals and goodness-of-fit parameter [25].

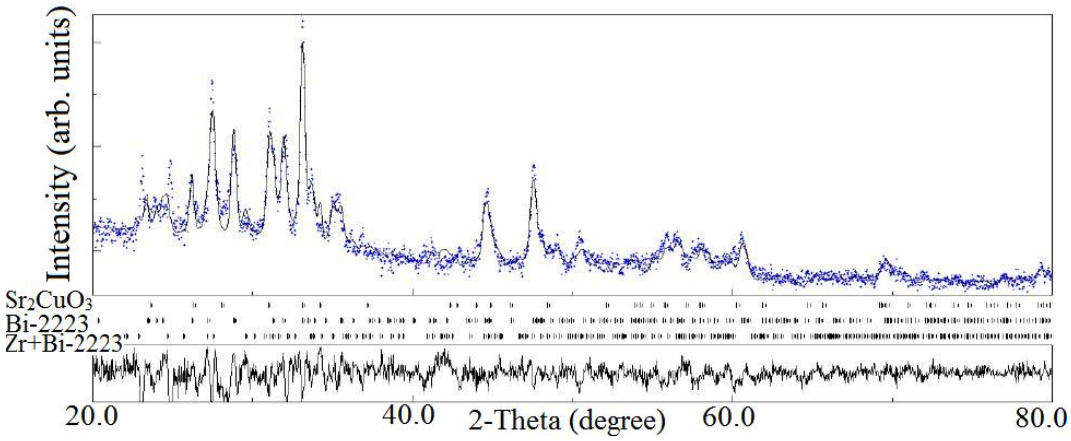


Fig. 1. XRD pattern and Rietveld refinement of the Bi-2223 sample with a nominal Zr content of x_{Zr} = 0.002 [25].

Blue dots represent the observed data, and the black solid line represents the calculated profile. Vertical tick marks indicate the Bragg positions of the Sr_2CuO_3, Bi-2223, and Bi-2223+Zr phases (from top to bottom). The difference profile (observed − calculated) is shown at the bottom and is vertically offset for clarity.

Figure 1 shows the XRD pattern and Rietveld refinement of the x_{Zr} = 0.002 sample. The pattern is predominantly consistent with the Bi-2223 phase (orthorhombic, space group A2aa). The refinement indicates 68.2 vol% of the Bi-2223+Zr phase (Bi-2223 in which Zr substitutes Cu), 26.2 vol% of the Bi-2223 phase, and a minor Sr_2CuO_3 secondary phase (5.6 vol%); no Bi-2212 phase was detected. No distinct reflections attributable to a crystalline Zr-containing secondary phase are resolved within the detection sensitivity of the present XRD measurement. Accordingly, the Bi-2223-type phases were taken as the principal crystalline phases in the analysis [25].

The refinement was performed with the MAUD software and yielded R_{wp} = 6.840%, R_{xp} = 4.111%, and a goodness-of-fit $S = R_{wp}/R_{xp}$ = 1.66. Within the adopted structural model, the refined Zr occupancy at the Cu(1) site of the Bi-2223+Zr phase is 0.0018, with a corresponding Cu(1) occupancy of 0.998. The refined Zr occupancy is close to the nominal value (x_{Zr} = 0.002), consistent with a very small Zr contribution at the modeled site [25].

Williamson–Hall analysis was subsequently performed to evaluate the contributions of crystallite size and lattice microstrain to the peak broadening, using $\beta \cos\theta/\lambda = K/D + \eta \sin\theta/\lambda$ with K = 1 [26, 27], where $y = \beta \cos\theta/\lambda$ and $x = \sin\theta/\lambda$. The intercept and slope of the linear fit give

the average crystallite size D and the microstrain η, respectively. Following the procedure reported previously by our group for this Bi-2223 system [25], the fit for the $x_{Zr} = 0.002$ sample is $y = 0.008x + 0.011$, corresponding to $\eta = 0.80 \pm 0.01\%$ and $D = 90.91 \pm 0.05$ nm. For comparison, the undoped sample reported in Ref. [25] gives $y = 0.003x + 0.015$, $\eta = 0.30 \pm 0.02\%$, and $D = 66.67 \pm 0.03$ nm [25].

Zr content (x)	Williamson-Hall equation	Microstrain η(%)	Crystallite size D (nm)
0	y=0.003x+0.015	0.3±0.02	66.67
0.002	y=0.008x+0.011	0.8±0.01	90.91

Table. 1. Williamson–Hall fitting parameters, microstrain, and crystallite size of the undoped and $x_{Zr} = 0.002$ Bi-2223 samples.

The comparison with the undoped sample shows that the introduction of a very small nominal Zr concentration ($x_{Zr} = 0.002$) is accompanied by an increase in the estimated microstrain from $0.30 \pm 0.02\%$ to $0.80 \pm 0.01\%$, together with an increase in the average crystallite size from 66.67 to 90.91 nm [25]. The increase in microstrain indicates a change in the local structural state and an increase in lattice distortion, while the increase in the Williamson–Hall crystallite size suggests a change in the coherent diffraction domain size. These results indicate that low-level Zr addition modifies the XRD peak broadening through simultaneous changes in microstrain and coherent crystallite size. Since the Williamson–Hall analysis is performed on the whole pattern, and the phase composition of the two samples differs (e.g., the Bi-2212 phase present in the undoped sample is absent at $x_{Zr} = 0.002$), these values should be regarded as effective parameters rather than properties of a single phase.

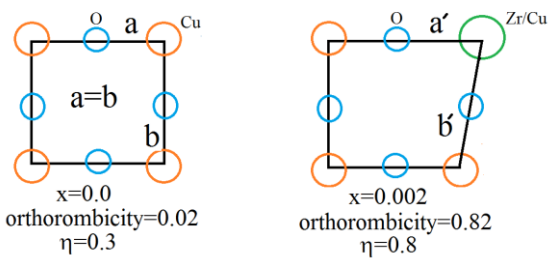


Fig. 2. Schematic illustration of a possible local structural perturbation associated with dilute Zr incorporation in the CuO_2 structural environment. The schematic is conceptual and does not represent the experimentally determined spatial distribution of Zr within the bulk sample.

Figure 2 provides a conceptual schematic of a possible local structural perturbation associated with dilute Zr incorporation in the CuO_2 structural environment. It is intended only to illustrate the possible effect of local cation substitution and does not represent the experimentally determined spatial distribution of Zr. In the structural refinement of the corresponding low-doped Zr/Cu-substituted Bi-2223 system, a small Zr occupancy was obtained at the modeled Cu(1) site, supporting the possibility of Zr incorporation at this site [25].

If Zr^{4+} is incorporated at a Cu-related site, the ionic radii of Zr^{4+} and Cu^{2+} are comparable for the relevant coordination environments [28], but their charge and electronic configuration differ (d^0 versus d^9), which can introduce local structural perturbations in the surrounding Cu–O framework. Such perturbations may modify the local Cu–O bonding environment and contribute to changes in the electronic and transport response of the CuO_2 planes. However, these effects should be regarded as a possible consequence of dilute Zr incorporation rather than direct evidence for a specific microscopic electronic mechanism. The present XRD and Williamson–Hall analyses thus indicate changes in the average structural parameters and microstrain.

3. Results and Discussion

3.1 Magnetic-field-dependent superconducting transition

The temperature-dependent electrical resistivity of the low-doped Zr/Cu-substituted Bi-2223 sample was measured under different applied magnetic fields of 0.3, 0.4, and 0.65 T. Figure 3 presents the normalized resistivity curves obtained under these magnetic fields. The measurements reveal the typical superconducting transition behavior of Bi-2223, including the normal metallic state at high temperatures, the superconducting transition region, and the low-temperature regime. The applied magnetic fields are much smaller than the upper critical fields reported for Bi-2223 materials [29]. Therefore, the observed field-dependent resistivity response should not be interpreted as the complete suppression of superconductivity. Instead, the applied

field modifies the measured resistivity transition and the low-temperature transport response of the polycrystalline sample.

The superconducting transition temperatures of the Bi-2223 samples were determined from their temperature-dependent electrical resistivity curves, as shown in Figure 3. For the undoped sample ($x_{Zr} = 0$), the onset, midpoint, and offset transition temperatures were determined to be 118 K, 110.5 K, and 105 K, respectively. With the addition of 0.002 Zr nanoparticles, the onset transition temperature slightly increased to 118.5 K, whereas the midpoint and offset transition temperatures decreased to 110.25 K and 102 K, respectively. Since a low-temperature resistivity increase was observed in the superconducting state, the offset transition temperature, T_c^{offset}, was adopted as the characteristic critical temperature for the subsequent calculations. Accordingly, $T_c = 105$ K and 102 K were used for the undoped and Zr-doped Bi-2223 samples, respectively.

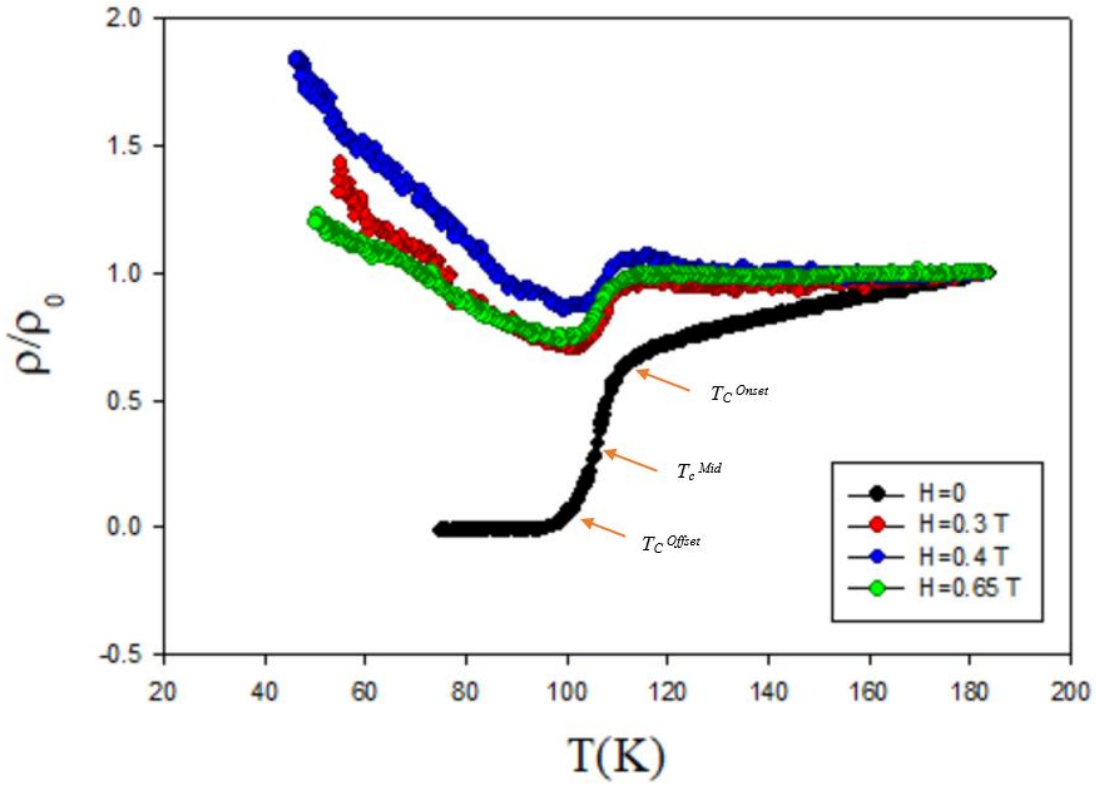


Fig. 3. Temperature dependence of the normalized resistivity of the low-doped Zr/Cu-substituted Bi-2223 sample measured under applied magnetic fields of 0.3, 0.4, and 0.65 T. The resistivity curves show a field-

dependent superconducting transition and a finite-resistance low-temperature regime in the polycrystalline sample.

Note. resistivity values at each magnetic field were normalized to the first resistivity value measured at the corresponding magnetic field.

3.2 Low-temperature resistivity anomaly in Zr/Cu-substituted Bi-2223

Below the superconducting transition, a finite and field-dependent resistivity persists in the low-temperature region of the low-doped Zr/Cu-substituted Bi-2223 sample, and the resistivity exhibits a minimum at T_{min} followed by an upturn on further cooling. In a polycrystalline type-II superconductor, finite resistivity under an applied field can arise from intergrain weak links and vortex-related dissipation [30]; such thermally activated contributions, however, decrease monotonically upon cooling. The resistivity upturn therefore points to an additional electronic scattering contribution, which is analyzed below in terms of Kondo-like scattering [11], with the characteristic temperature scale of the sample, $T_K^{ex} \approx$ 98.5 K, obtained from the experimental data (Section 3.5).

3.2.1 Zeeman Energy

The applied magnetic fields used in this study (0.3–0.65 T) are significantly smaller than the upper critical field reported for Bi-2223 [29]. The corresponding Zeeman energy, $E_Z = g\mu_B B$, was estimated for the maximum field of 0.65 T assuming $g = 2$, giving $E_Z \approx 0.075$ meV. This value is about two orders of magnitude smaller than the thermal energy scale associated with the superconducting transition, $k_B T_c^{offset} \approx 8.8$ meV ($T_c^{offset} = 102$ K), and also than the characteristic Kondo-like energy scale, $k_B T_K^{ex} \approx 8.5$ meV ($T_K^{ex} \approx 98.5$ K). Since the Kondo resonance is expected to split only when $g\mu_B B$ becomes comparable to $k_B T_K$, the field is not expected to split or quench the Kondo-like scattering in this field range.

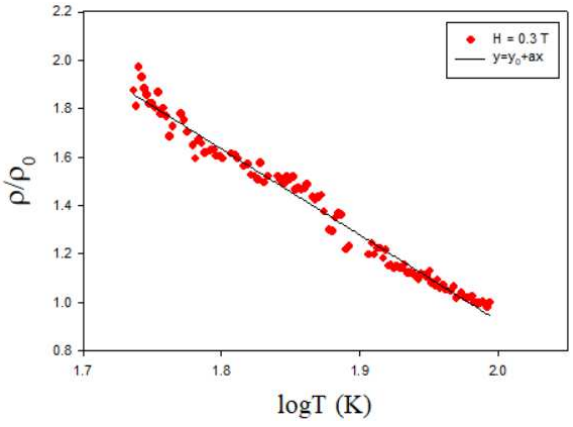
3.2.2 Vortex-related contribution to the finite resistivity

Finite resistivity under an applied magnetic field is expected in a polycrystalline type-II superconductor and may arise from vortex motion, flux creep, and weak intergrain coupling [30, 31]. To estimate this contribution, an Arrhenius analysis of the form $\rho = \rho_0 \exp(-U/k_B T)$ was performed. The extracted activation energies, $U/k_B \approx$ 72.52, 63.16, and 44.85 K (≈ 6.25, 5.44, and 3.86 meV) for 0.3, 0.4, and 0.65 T, respectively, decrease with increasing field, consistent with a reduced effective pinning barrier and enhanced vortex mobility at higher fields [31].

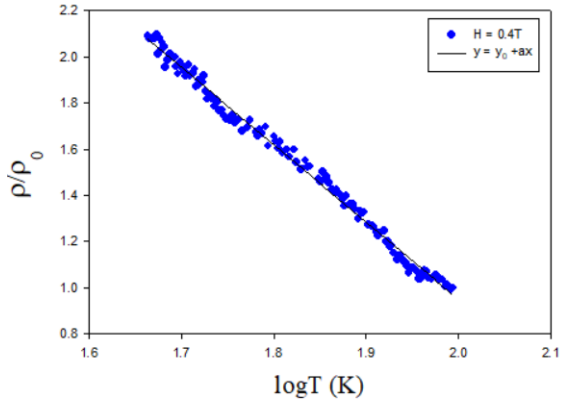
Because this thermally activated term decreases monotonically upon cooling, it cannot account for the resistivity upturn below T_{min}, which has the opposite temperature dependence. Instead, the approximately linear dependence of the normalized resistivity on ln T, together with the agreement between the experimental logarithmic coefficient and the Kondo-like scattering model, supports the attribution of the upturn to Kondo-like scattering [7, 11, 32].

3.3 Analysis of Kondo-like scattering contribution

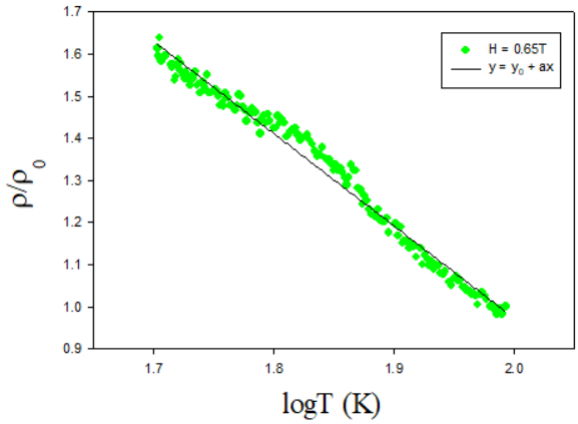
The logarithmic temperature dependence observed in the low-temperature resistivity provides a phenomenological basis for considering Kondo-like scattering as a possible contribution to the observed transport behavior. To further examine this logarithmic temperature dependence, the normalized resistivity was replotted as a function of logT within the finite-resistance low-temperature regime. For each applied magnetic field, the resistivity was normalized to the first measured resistivity value in the corresponding low-temperature region, denoted by ρ_0. As shown in Figure 4, the normalized resistivity exhibits an approximately linear dependence on logT over the investigated temperature range for all three applied magnetic fields.



a=0.3 T



b= 0.4 T



c= 0.65T

Fig. 4. Normalized resistivity plotted as a function of logT for the Zr/Cu-substituted Bi-2223 sample under applied magnetic fields of (a) 0.3, (b) 0.4, and (c) 0.65 T. The resistivity at each magnetic field was normalized to the first measured resistivity value in the corresponding low-temperature region ρ_0.

The experimental data were fitted using the linear relation $y = y_0 + ax$, where y_0 is the intercept and a is the coefficient describing the logarithmic temperature dependence of the normalized resistivity. The linear fits yield coefficients of determination of $R^2 = 0.98$, 0.99, and 0.98 for 0.3, 0.4, and 0.65 T, respectively. The corresponding standard errors are 0.0398, 0.0294, and 0.0259. These results demonstrate that the normalized low-temperature resistivity follows a pronounced linear dependence on logT over the investigated temperature interval.

Such a logT dependence in consistent with the interpretation of the observed low-temperature resistivity upturn in terms of Kondo-like scattering. In this system, Zr substitution is not assumed to introduce a conventional localized magnetic moment directly. Instead, the substitution may locally perturb the Cu–O electronic environment and modify the spin correlations of neighboring Cu sites. Theoretical studies have shown that non-magnetic impurities in cuprates can induce local magnetic moments on nearby Cu sites under appropriate

electronic conditions, and such impurity-induced moments have been discussed in connection with Kondo-like behavior [19, 32]. Therefore, impurity-induced spin fluctuations provide a physically plausible, although not experimentally verified in the present sample, mechanism for an additional magnetic scattering channel.

Importantly, the applied magnetic field is not considered to generate the Kondo-like scattering state. Rather, the field drives the polycrystalline sample into a finite-resistance mixed-state regime by weakening intergrain superconducting transport and promoting vortex-related dissipation. This finite-resistance regime enables the temperature dependence of the underlying electronic scattering contribution to be examined. The observation of a systematic logT dependence at all three applied fields is therefore the principal transport observation supporting a Kondo-like scattering contribution, rather than evidence that the magnetic field itself creates the Kondo state.

3.4 Theoretical framework for Kondo-like scattering (ρ_{spin})

The parameters used in the present Kondo-inspired phenomenological model were defined according to the local electronic structure and the multilayer nature of the Bi-2223 superconducting host. The resistivity contribution associated with spin-dependent scattering can be described within the second-order perturbation approach originally developed for Kondo systems [7]:

$$\rho_{spin} = c\rho_M \left\{1 + \left(\frac{3\, Z_{eff}\, J_{ex}}{\varepsilon_F}\right) log\, T\right\} \quad (1)$$

Here, c is the impurity concentration, Z_{eff} represents the effective number of conducting CuO_2 layers included in the present phenomenological description, ε_F is the Fermi energy, and J_{ex} is defined as an effective exchange-like coupling between the impurity-induced local spin fluctuations of the perturbed Cu–O host and the conducting quasiparticles of the CuO_2 planes. J_{ex} may be positive ($J_{ex} > 0$, ferromagnetic alignment) or negative ($J_{ex} < 0$, favoring antiferromagnetic alignment). While both may be present, Kondo showed that only the antiferromagnetic exchange leads to the characteristic logarithmic increase in resistivity. The prefactor (ρ_M) is defined as [7]:

$$\rho_M = \frac{3\pi\, m\, J_{ex}^2\, s(s+1)(V_{cell})}{2e^2\, \hbar \varepsilon_F} \quad (2)$$

Where m is the electron mass, s is the spin quantum number of the impurity, V_{cell} is the unit-cell volume. Since the present system is a periodic multilayer superconducting structure, its electronic and structural properties are naturally described in terms of the crystallographic unit cell rather than an isolated host atom. The total resistivity can be expressed as the sum of three contributions: lattice resistivity (ρ_L), impurity potential scattering (ρ_A), and the Kondo-like scattering term with a logarithmic temperature dependence [7].

$$\rho_{Total} = \rho_L + c\rho_A + c\rho_M + c\left(\frac{3\, Z_{eff}\, J_{ex}\, \rho_M}{\varepsilon_F}\right) \log T \tag{3}$$

The effective impurity concentration in these equations can thus be considered proportional to the Zr doping level. Since an applied magnetic field can induce local moments around nonmagnetic impurities [20], and exchange interactions in layered systems can be tuned by external fields [33], the field is treated here as an external parameter controlling the strength of the Kondo-like scattering.

3.4.1 Calculation of spin-exchange coupling

The spin-exchange coupling in Zr/Cu-substituted Bi-2223 can be calculated with some modification using the Abrikosov-Gorkov (AG) theory and considering the method used in the reference [34]. The following equation is based on different doping values.

$$T_C / T_{C_0} = \mathrm{t} \tag{4}$$

$$\frac{d(t)}{dn_I}_{n_{I\to 0}} = \frac{d(t)}{dx}_{x\to 0} = \frac{-\pi^2\, N(\varepsilon_F)\, J_{ex}^2\, (g-1)^2\, J(J+1)}{2K_B}$$

Where t is the normalized temperature to the transition temperature without impurity ($T_{C_0}^{Offset}$ = 105 K, when H = 0, and x_{Zr} = 0), x is the amount of impurity, g is the Lande coefficient, J is the total angular momentum, $N(\varepsilon_F)$ is the density of states at the Fermi level, and K_B is Boltzmann's constant.

Since the Kondo-like scattering contribution was observed only for the Zr concentration of 0.002, corresponding to $Bi_{1.66}Pb_{0.34}Sr_2Ca_2Cu_{2.998}Zr_{0.002}O_{10+\delta}$, Eq. (4) was evaluated for the

applied magnetic fields used in the resistivity measurements. The impurity concentration was therefore kept constant, while the magnetic field was treated as an external parameter that can modify the magnetic-scattering contribution. Because no direct magnetic measurement was performed, the calculations are interpreted phenomenologically in terms of field-dependent Kondo-like scattering. In this framework, the factor $[(g-1)^2 J(J+1)]$ represents the effect of the magnetic field. J_{ex} is calculated based on the change in the applied magnetic field in Tesla.

$$\frac{d(t)}{dH} = \frac{-\pi^2 N(\varepsilon_F) J_{ex}^2 H}{2K_B} \tag{5}$$

Here, H is the applied magnetic field in Tesla, $N(\varepsilon_F)$ is the density of state at the Fermi level. The density of states at the Fermi level was taken as $N(\varepsilon_F) = 0.44$ (states.ev^{-1}.atom^{-1}), corresponding to the Cu(1)-projected (d)-state DOS. This choice is consistent with the structural determination that Zr preferentially substitutes for Cu at the Cu(1) site. Therefore, the Cu(1)-derived (d)-states provide a physically relevant representation of the local host electronic states associated with the substitutional Zr site. The value of 0.44 (states/ev.atom) was adopted from the reported Cu(1)-(d) electronic-structure calculation for the Bi-2223 system and was used as a reasonable estimate of the local DOS at the Fermi level [35]. This approach provides a more physically meaningful estimation because the inner and outer CuO_2 planes in Bi-2223 are not electronically equivalent and possess different local electronic environments.

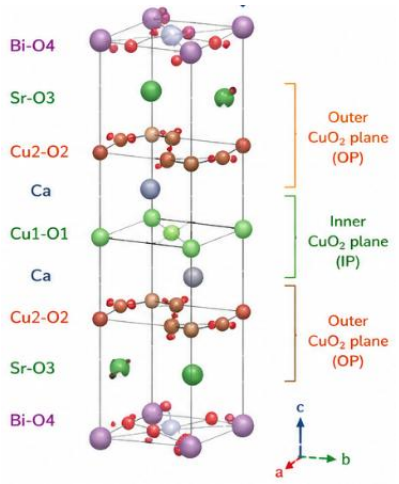


Fig. 5. Unit cell structure of Bi-2223

The slope of Eq. (5) for 0.3, 0.4 , and 0.65 T are -0.0198 T^{-1}, -0.0237 T^{-1}, -0.0284 T^{-1}, respectively. All temperatures are normalized at three different magnetic fields (0.3, 0.4, and 0.65 T) with respect to the transition temperature of the impurity-free superconducting sample in zero magnetic field, i.e., 105 K. Substituting these values into Eq. 5 yields exchange constants of -1.618 meV, -1.533 meV, and -1.316 meV for fields of 0.3, 0.4, and 0.65 T, respectively. The negative sign confirms antiferromagnetic spin alignment, consistent with Kondo's original interpretation.

3.4.2 Effective energy scale

In conventional metals, the Fermi energy ε_F serves as the characteristic energy scale for electron scattering. However, in the superconducting state of strongly correlated cuprates, the low-energy electronic excitations are governed by the superconducting gap due to the opening of the gap and the accompanying reconstruction of the electronic density of states near the Fermi level [36]. Therefore, for low-energy Kondo-like scattering in the superconducting phase, the superconducting gap (Δ) can be regarded as the appropriate effective energy scale instead of ε_F. Since Bi-based cuprate superconductors exhibit strong-coupling superconductivity, the gap was estimated using the experimentally reported scaling relation ($2\Delta \approx 8k_B T_C$) [37] which has been observed in high temperature cuprate superconductors including Bi-based compounds. For ($T_C{}^{offset}$ = 102 K, when X 0, and x_{Zr} = 0.002), this gives $2\Delta \approx 70$ meV, and $\Delta \approx 35$ meV, which was adopted as the characteristic energy scale in the present analysis.

3.4.3 Z_{eff} and V_{cell} calculation

Because Zr/Cu-substituted Bi-2223 is a multilayer cuprate consisting of three electronically active CuO_2 planes, the conventional host parameter (z) was replaced by an effective layer parameter, (Z_{eff}). We set (Z_{eff}=3) to account for the three CuO_2 conducting planes constituting the superconducting electronic subsystem.

Furthermore, the effective volume parameter was taken as the crystallographic unit-cell volume, $V_{cell} = abc$, where (a = 5.713Å), (b = 5.807Å), and (c = 38.860 Å) are the lattice parameters of the Zr/Cu-substituted Bi-2223 structure. The value of V_{cell} is 1289.196 $Å^3$ or 1.289×10^{-21} cm^3.

3.4.4 Final calculation

The value of ρ_M for fields of 0.3, 0.4, and 0.65 T is obtained from Eq. 2 as 18.39×10^{-3} Ωcm, 16.508×10^{-3} Ωcm, and 12.168×10^{-3} Ωcm, respectively, using the corresponding J_{ex} values. Substituting these results into Eq.1 yields the spin-scattering resistivity ρ_{spin} for each field.

P_L is zero in the superconducting region, ρ_A (arising from unwanted phases) has a negligible effect on Kondo-like scattering, and the total resistivity reduces to: ($\rho_T = \rho_{spin}$). Thus, for Zr/Cu-substituted Bi-2223, the normalized resistivity based on the Kondo-like equations for applied external magnetic fields of 0.3, 0.4, and 0.65 T, below 102 K, is obtained with the following equations, respectively. Each dataset was normalized to the initial resistivity value for the corresponding magnetic field.

$$\frac{\rho_{spin}(estimated)}{\rho_0(estimated)} = 3.678 - 1.533\, log\, T \tag{6}$$

$$\frac{\rho_{spin}\,(estimated)}{\rho_0(estimated)} = 3.301 - 1.304\ \ log\, T \tag{7}$$

$$\frac{\rho_{spin}\,(estimated)}{\rho_0(estimated)} = 2.433 - 0.825\, log\, T \tag{8}$$

Fitting Eq. 9 to the experimental data below 102K in Zr/Cu-substituted Bi-2223 define the experimental resistivity for 0.3, 0.4, and 0.65 T, respectively.

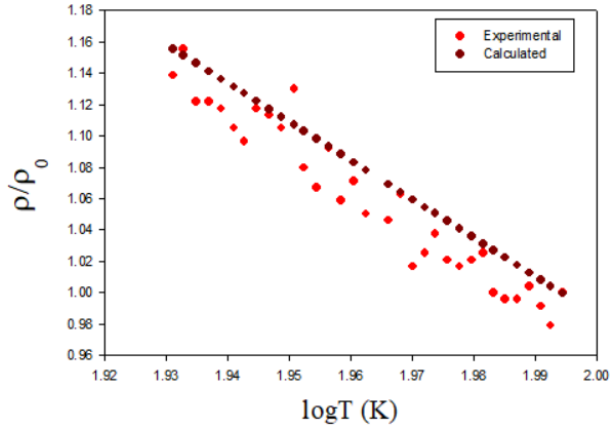
$$\rho_{spin}(experimental) = \ \rho_0 - A\, log\, T \tag{9}$$

$$\frac{\rho_{spin}(experimental)}{\rho_0(experimental)} = 2.999 - 1.327\, log\, T \tag{10}$$

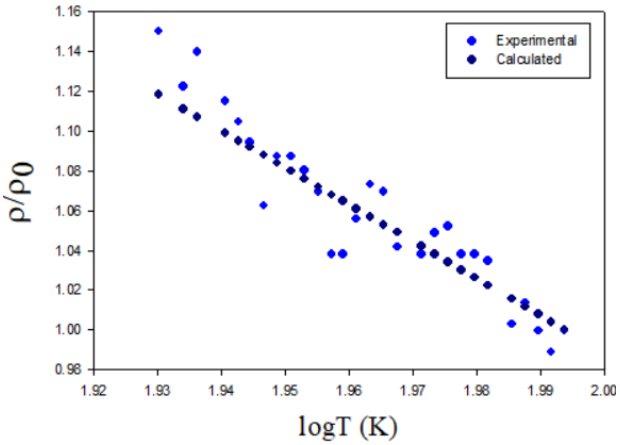
$$\frac{\rho_{spin}(experimental)}{\rho_0(experimental)} = \ 3.431 - 1.503\, log\, T \tag{11}$$

(12)

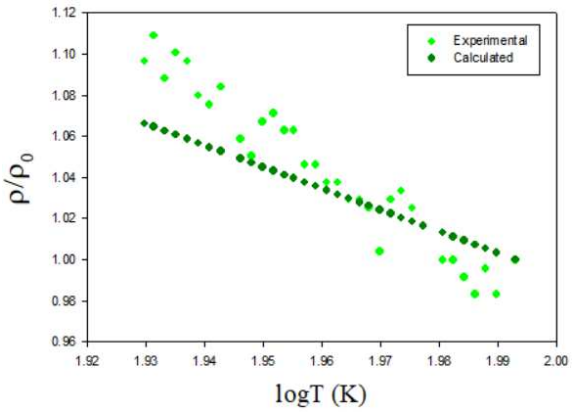
$$\frac{\rho_{spin}(experimental)}{\rho_0(experimental)} = 2.004 - 0.820\, log\, T$$



a= 0.3 T



b= 0.4 T



c= 0.65T

Fig 6. Comparison of experimental and estimated ρ_{spin} for each magnetic field

As shown in Figure 6, the agreement between the experimental and estimated ρ_{spin} was assessed from the overall trend of the two curves over the fitted temperature range, rather than from any single fitting parameter. At 0.3 T (Fig. 6a), the experimental resistivity values are lower than those calculated from Eq. (6), resulting in a relatively limited agreement. At 0.4 T (Fig. 6b), the experimental and calculated curves follow the same trend and show the closest agreement among the investigated fields; this is also the field with the highest linearity in the log T fit ($R^2 = 0.99$). At 0.65 T (Fig. 6c), the logarithmic coefficients are nearly identical ($A_{ex} = 0.820$, $A_{cal} = 0.825$), but the experimental values lie below the calculated ones ($\rho_0 = 2.004$ versus 2.433), so the two curves are offset and the trend is not reproduced as well as at 0.4 T. Thus, among the three applied fields, 0.4 T provides the best overall agreement between the Kondo-like scattering model and the experimental data. This observation is interpreted as a field-dependent variation in the relative contribution of the Kondo-like scattering term to the measured resistivity.

The experimental and calculated parameters are summarized in Table 2. The comparison between the experimental and estimated values shows that the agreement depends on the applied magnetic field and on the parameter considered. At 0.3 T, the experimental and calculated values of ρ_0 are 2.999 and 3.678, respectively, while the corresponding values of A are 1.327 and 1.533. At 0.4 T, the calculated value of ρ_0 3.301 is in close agreement with the experimental value 3.431, whereas the corresponding values of A are 1.304 and 1.503, respectively. At 0.65 T, the agreement between the experimental and calculated logarithmic coefficients is particularly close, with (A^{ex} =0.820) and (A^{cal} =0.825) , while the corresponding values of ρ_0 are 2.004 and 2.433. These results support the applicability of the proposed Kondo-like scattering expression as a phenomenological description of the low-temperature resistiviy.

$H(T)$	$T_{min}(K)$	$\rho_{min}(\Omega cm)$	$T_K^{ex}(K)$	$J_{ex}(meV)$	ρ_0^{ex}	ρ_0^{cal}	A^{ex}	A^{cal}
0.3	100.39	3.63E-05	98.72	-1.618	2.999	3.678	1.327	1.533
0.4	99.40	4.35E-05	98.56	-1.533	3.431	3.301	1.503	1.304
0.65	98.83	3.65E-05	98.41	-1.316	2.004	2.433	0.820	0.825

Table. 2. Summary of the minimum temperatures, and resistivity, experimental and calculated logarithmic coefficients, Kondo temperature, and spin-exchange parameter for Zr/Cu-substituted Bi-2223 at magnetic fields of 0.3, 0.4, and 0.65 T.

Note: T_{min} represents the temperature at which the minimum resistance ρ_{min} expressed in (**Ω**cm) is observed, marking the onset of the Kondo-like scattering. T_K denotes the Kondo temperature. Experimental and calculated values of the logarithmic coefficients and spin-exchange parameter are compared across the investigated magnetic fields.

3.5. Kondo temperature

The low-temperature resistivity behavior of the Zr/Cu-substituted Bi-2223 at magnetic fields of 0.3, 0.4, and 0.65 T was further analyzed in terms of a Kondo-like contribution. The minimum resistivity, T_{min}, was determined from the experimental $\rho(T)$curves at each applied magnetic field, and the corresponding Kondo temperature, $T_K{}^{ex}$, was extracted from the resistivity analysis. The extracted values of T_{min} and $T_K{}^{ex}$, together with the corresponding minimum resistivity $\rho_{\min}$, are summarized in Table 2.

At (H=0.3T, 0.4 T,and 0.65 T), T_{min} decreases from 100.39 to 99.40 and 98.83 K, respectively, while $T_K{}^{ex}$ decreases from 98.72 to 98.56 and 98.41 K. Thus, both characteristic temperatures exhibit a systematic decrease with increasing magnetic field.

Many methods have been proposed for calculating the classical Kondo temperature, such as the Hamann method. However, the conventional Hamann formalism cannot be directly applied because it was developed for dilute magnetic impurities in a conventional Fermi-liquid host [38], whereas cuprate superconductors exhibit strongly correlated and non-Fermi-liquid behavior [39].

Nevertheless, Kondo-like resistivity upturns have been reported in cuprates even for nonmagnetic impurities, where impurity-induced local magnetic moments can give rise to Kondo-like scattering [11, 32].

4. Conclusions

1. In this work, the low-temperature transport behavior of lightly Zr/Cu-substituted Bi-2223 high-temperature superconductors was investigated under weak magnetic fields. The results reveal a logarithmic contribution to the low-temperature resistivity in the superconducting low-temperature regime, which is consistently described as a Kondo-like scattering contribution.

2. Structural refinement indicates the presence of Zr at a very low substitution level (x_{Zr} = 0.002) in the Bi-2223 sample, with no additional crystalline phase attributable to Zr detected within the sensitivity of the XRD analysis. The associated lattice distortion and microstrain provide evidence of local structural disorder, which may perturb the local Cu–O electronic environment and contribute to the observed anomalous transport behavior.

3. Although Zr^{4+} is not expected to carry an intrinsic localized magnetic moment, its substitution for Cu can perturb the local Cu–O electronic environment and spin correlations. Such impurity-induced modifications may provide a source of localized or fluctuating spin degrees of freedom on neighboring Cu sites, which can contribute to spin-dependent scattering of itinerant carriers. In the absence of direct magnetic measurements, this mechanism is considered a possible microscopic origin of the observed Kondo-like transport contribution rather than a directly established magnetic state.

4. Under applied magnetic fields, a finite-resistance regime develops below the superconducting transition. The Arrhenius analysis yields activation energies of approximately 6.25, 5.44, and 3.86 meV at 0.3, 0.4 , and 0.65 T, respectively, indicating a field-dependent thermally activated resistive background associated with mixed-state dissipation. Such behavior is compatible with vortex motion, flux creep, and weak intergrain coupling in the polycrystalline material. Importantly, however, the characteristic low-temperature anomaly exhibits an approximately linear dependence on log(T), with coefficients of determination of R^2 = 0.98, 0.99, and 0.98 for 0.3, 0.4, and 0.65 T, respectively. The systematic logarithmic temperature dependence, together with the comparison with the theoretical spin-scattering expression, provides transport-based evidence for an additional Kondo-like scattering contribution.

5. The theoretical analysis provides further quantitative support for the Kondo-like interpretation. The effective exchange parameter J_{ex} obtained from the model is negative for all investigated fields, with values of −1.618, −1.533, and −1.316 meV at 0.3, 0.4, and 0.65 T, respectively. The negative sign corresponds to antiferromagnetic exchange within the adopted Kondo framework.

6. The Kondo temperature was determined from experimental data; it was observed that the Kondo temperature decreases slightly as the magnetic field increases. Additionally, consistent with the Kondo model, for Zr/Cu-substituted Bi-2223, a single

Kondo temperature is expected; for our material, the Kondo temperature is 98.5 K to a very good approximation.

7. The comparison between the experimental and calculated results shows that the best overall agreement is obtained at 0.4 T, where the two resistivity curves follow the same trend and the log T fit has its highest coefficient of determination ($R^2 = 0.99$). At 0.65 T the logarithmic coefficients agree closely, but the curves remain offset.

8. Overall, the results support a picture in which dilute Zr substitution modifies the local structural and electronic environment of Bi-2223 and introduces an additional logarithmic spin-dependent scattering channel that becomes observable within the finite-resistance mixed-state regime. The present findings therefore provide transport-based evidence for **Kondo-like scattering in lightly Zr/Cu-substituted Bi-2223**, while not implying the formation of a conventional magnetic-impurity Kondo system, a Kondo lattice, or field-induced magnetic moments. Further experimental investigations, particularly local magnetic probes, spectroscopic measurements, and systematic studies over a broader Zr concentration and magnetic-field range, would be valuable for directly testing the proposed impurity-induced spin-fluctuation mechanism and establishing its microscopic origin.

5. Funding Declaration

This research received no specific grant from any national or international funding agency in the public, commercial, or not-for-profit sectors. The research expenses were covered by the students through personal resources and student discounts (e.g., for XRD measurements), with occasional personal support from the corresponding author for purchasing materials.

6. Data availability

The datasets generated and analysed during the current study are available from the corresponding author on reasonable request.

7. References

1. Dagotto, E. Correlated electrons in high-temperature superconductors. Rev. *Mod. Phys*. **66**, 763–840 (1994). https://doi.org/10.1103/RevModPhys.66.763

2. Keimer, B., Kivelson, S. A., Norman, M. R., Uchida, S. & Zaanen, J. From quantum matter to high-temperature superconductivity in copper oxides. *Nature* **518**, 179–186 (2015). https://doi.org/10.1038/nature14165

3. Bednorz, J. G. & Müller, K. A. Possible high Tc superconductivity in the Ba–La–Cu–O system. Z. *Phys. B* **64**, 189–193 (1986). https://doi.org/10.1007/BF01303701

4. Fisk, Z. & Sarrao, J. L. The new generation high-temperature superconductors. Annu. Rev. *Mater. Sci*. **27**, 35–67 (1997). https://doi.org/10.1146/annurev.matsci.27.1.35

5. Hussey, N. E. Phenomenology of the normal-state in-plane transport properties of high-Tc cuprates. *J. Phys.: Condens. Matter* **20**, 123201 (2008) .https://doi.org/10.1088/0953-8984/20/12/123201

6. Blatter, G., Feigel'man, M. V., Geshkenbein, V. B., Larkin, A. I. & Vinokur, V. M. Vortices in high-temperature superconductors. *Rev. Mod. Phys.* **66**, 1125–1388 (1994). https://doi.org/10.1103/RevModPhys.66.1125

7. Kondo, J. Resistance minimum in dilute magnetic alloys. *Prog. Theor. Phys.* **32**, 37–49 (1964). https://doi.org/10.1143/PTP.32.37

8. Wilson, K. G. The renormalization group: Critical phenomena and the Kondo problem. Rev. *Mod. Phys*. **47**, 773–840 (1975). https://doi.org/10.1103/RevModPhys.47.773

9. Stewart, G. R. Heavy-fermion systems. Rev. *Mod. Phys.* **56**, 755–787 (1984). https://doi.org/10.1103/RevModPhys.56.755

10. Gegenwart, P., Si, Q. & Steglich, F. Quantum criticality in heavy-fermion metals. *Nat. Phys.* **4**, 186–197 (2008). https://doi.org/10.1038/nphys892

11. Bobroff, J. et al. Spinless impurities in high-Tc cuprates: Kondo-like behavior. *Physical Review* Letters **83**, 4381 (1999). https://doi.org/10.1103/PhysRevLett.83.4381

12. Balatsky, A. V., Vekhter, I. & Zhu, J.-X. Impurity effects in conventional and unconventional superconductors. Rev. *Mod. Phys*. **78**, 373–433 (2006). https://doi.org/10.1103/RevModPhys.78.373

13. Cava, R. J. et al. Bulk superconductivity at 91 K in single-phase oxygen-deficient perovskite $Ba_2YCu_3O_{9-\delta}$. *Phys. Rev. Lett.* **58**, 1676–1679 (1987). https://doi.org/10.1103/PhysRevLett.58.1676

14. Damascelli, A., Hussain, Z. & Shen, Z.-X. Angle-resolved photoemission studies of the cuprate superconductors. Rev. *Mod. Phys*. **75**, 473–541 (2003). https://doi.org/10.1103/RevModPhys.75.473

15. Alloul, H., Bobroff, J., Gabay, M. & Hirschfeld, P. J. Defects in correlated metals and superconductors. *Rev. Mod. Phys.* **81**, 45–108 (2009). https://doi.org/10.1103/RevModPhys.81.45

16. Gupta, S., Mazumdar, C., Padalia, B. D., Prakash, O., Nagarajan, R., Gupta, L. C. & Pattanaik, A. K. On Zr substitution in T′-type Nd–Ce–Cu–O system. *Mod. Phys. Lett. B* **14**, 415–422 (2000). https://doi.org/10.1142/S0217984900000598
17. Saritekin, N. K., Terzioglu, C., Pakdil, M., Turgay, T. & Yildirim, G. Solubility limit of tetravalent Zr nanoparticles in Bi-2223 crystal lattice and evaluation of fundamental characteristic properties of new system. *Journal of Materials Science: Materials in Electronics* **27**, 1854–1865 (2016). https://doi.org/10.1007/s10854-015-3964-5
18. Yildirim, G., Akdogan, M., Altintas, S. P., Erdem, M., Terzioglu, C. & Varilci, A. Investigation of the magnetic field angle dependence of resistance, irreversibility field, upper critical field and critical current density in DC sputtered Bi-2223 thin film. *Physica B: Condensed Matter* **406**, 1853–1857 (2011). https://doi.org/10.1016/j.physb.2011.02.041
19. Chen,Y. & Ting, C. S. States of local moment induced by nonmagnetic impurities in cuprate superconductors. Physical Review Letters 92, 077203 (2004). https://doi.org/10.1103/PhysRevLett.92.077203
20. Gabay, M., Semel, E., Hirschfeld, P. J. & Chen, W. Field-induced local moments around nonmagnetic impurities in metallic cuprates. *Physical Review B* **77**, 165110 (2008). https://doi.org/10.1103/PhysRevB.77.165110
21. Shahbaz Tehrani, F. & Daadmehr, V. Superconductivity versus structural parameters in calcium-doped $Nd_{1-x}Ca_xFeAsO_{0.8}F_{0.2}$ superconductors. *J. Supercond. Nov. Magn.* **33**, 337–345 (2020). https://doi.org/10.1007/s10948-019-05365-6
22. Ozturk, O., Yegen, D., Yilmazlar, M., Varilci, A. & Terzioglu, C. The effect of cooling rates on properties of $Bi_{1.7}Pb_{0.35}Sr_{1.9}Ca_{2.1}Cu_3O_\gamma$ superconductors produced by solid-state reaction method. *Physica C* **451**, 113–117 (2007). https://doi.org/10.1016/j.physc.2006.11.003
23. Darsono, N., Yoon, D.-H. & Raju, K. Effects of the sintering conditions on the structural phase evolution and T_C of $Bi_{1.6}Pb_{0.4}Sr_2Ca_2Cu_3O_7$ prepared using the citrate sol–gel method. *J. Supercond. Nov. Magn.* **29**, 1491–1497 (2016). https://doi.org/10.1007/s10948-016-3459-5
24. Zarabinia, N., Daadmehr, V., Tehrani, F. S. & Abbasi, M. Influence of Ag/Cu substitution on structural effect of new high temperature superconductor $Y_3Ba_5Cu_8O_{18}$. *Procedia Mater. Sci. **11**, 242–247 (2015).* https://doi.org/10.1016/j.mspro.2015.11.125
25. Vafajoo, S., Daadmehr, V. & Tehrani, S. Investigation of Zr nanoparticle effects on structural phase stability, micro strains, and flux pinning in BSCCO-Zr/Cu doped HTSC. *J. Interfaces Thin Films Low Dimens. Syst.* **5**, 479–492 (2022). https://doi.org/10.22051/jitl.2023.42264.1076

26. Bantikatla, H., Devi, L. N. S. M. P. & Bhogoju, R. K. Microstructural parameters from X-ray peak profile analysis by Williamson-Hall models: A review. *Mater. Today Proc.* **47**, 4891–4896 (2021). https://doi.org/10.1016/j.matpr.2021.06.256

27. Williamson, G. K. & Hall, W. H. X-ray line broadening from filed aluminium and wolfram. *Acta Metallurgica* **1**, 22–31 (1953). https://doi.org/10.1016/0001-6160(53)90006-6

28. Shannon, R. D. Revised effective ionic radii and systematic studies of interatomic distances in halides and chalcogenides. *Acta Crystallogr. Sect. A* **32**, 751–767 (1976). https://doi.org/10.1107/S0567739476001551

29. Matsubara, I., Tanigawa, H., Ogura, T., Yamashita, H., Kinoshita, M. & Kawai, T. Upper critical field and anisotropy of the high-Tc $Bi_2Sr_2Ca_2Cu_3O_x$ phase. *Physical Review B* **45**, 7414–7417 (1992). https://doi.org/10.1103/PhysRevB.45.7414

30. Horvat, J., Guo, Y. C. & Dou, S. X. Formation of weak and strong links in Ag/Bi-2223 superconducting tapes. *Physica C* **271**, 59–66 (1996). https://doi.org/10.1016/S0921-4534(96)00503-5

31. . Palstra, T. T. M., Batlogg, B., van Dover, R. B., Schneemeyer, L. F. & Waszczak, J. V. Dissipative flux motion in high-temperature superconductors. *Physical Review B* **41**, 6621 (1990). https://doi.org/10.1103/PhysRevB.41.6621

32. Park, K. Kondo effect of nonmagnetic impurities and coexisting charge order in cuprate superconductors. *Physical Review B* **67**, 094513 (2003). https://doi.org/10.1103/PhysRevB.67.094513

33. Bi, X., Qiu, C., Qin, F., Huang, J. & Yuan, H. Controlling exchange interactions and emergent magnetic phenomena in layered 3d-orbital ferromagnets. *Adv. Phys. Res*. **2**, 2200106 (2023). https://doi.org/10.1002/apxr.202200106

34. Shahbaz Tehrani, F. & Daadmehr, V. The superconductivity mechanism in Nd-1111 iron-based superconductor doped by calcium. *J. Low Temp. Phys.* **199**, 1299–1313 (2020). https://doi.org/10.1007/s10909-020-02418-1

35. Camargo-Martínez, J. A., Espitia, D. & Baquero, R. First-principles study of electronic structure of $Bi_2Sr_2Ca_2Cu_3O_{10}$. *J. Appl. Phys.* **114**, 183904 (2013). https://doi.org/10.1063/1.4826446

36. Hashimoto, M., Vishik, I. M., He, R.-H., Devereaux, T. P. & Shen, Z.-X. Energy gaps in high-transition-temperature cuprate superconductors. *Nature Physics* **10**, 483–495 (2014). https://doi.org/10.1038/nphys3009

37. Anzai, H., Ino, A., Arita, M., Namatame, H., Taniguchi, M., Ishikado, M., Fujita, K., Ishida, S. & Uchida, S. Relation between the nodal and antinodal gap and critical temperature in superconducting Bi2212. *Nat. Commun.* **4**, 1815 (2013). https://doi.org/10.1038/ncomms2805

38. Zeng, H., Zhou, D., Liang, G., Tang, R., Hang, Z. H., Hu, Z., Pei, Z. & Ling, X. S. Kondo effect and superconductivity in niobium with iron impurities. *Sci. Rep*. **11**, 14256 (2021). https://doi.org/10.1038/s41598-021-93731-6

39. Rullier-Albenque, F., Alloul, H., Balakirev, F. & Proust, C. Disorder, Metal-Insulator crossover and Phase diagram in high-T_C cuprates. *Europhys. Lett*. **81**, 37008 (2008). https://doi.org/10.1209/0295-5075/81/37008